Density functional calculations of the formation and migration enthalpies of monovacancies in Ni: Comparison of local and nonlocal approaches

El Hocine Megchiche, Simon Perusin, Jean-Claude Barthelat, Claude Mijoule

Density functional calculations of the formation and migration enthalpies of monovacancies in Ni: Comparison of local and nonlocal approaches

El Hocine Megchiche,[1,2] Simon Pérusin,[3] Jean-Claude Barthelat,[1] and Claude Mijoule[3,*]

[1]*Laboratoire de Physique Quantique, IRSAMC (UMR 5626), Université Paul Sabatier, 118 Route de Narbonne, 31062, Toulouse Cedex 4, France*

[2]*Laboratoire de Physique et Chimie Quantique (LPCQ), Université Mouloud Mammeri, Tizi-Ouzou, Algeria*

[3]*CIRIMAT UMR CNRS/INP/UPS, Ecole Nationale d'Ingénieurs en Arts Chimiques et Technologiques (ENSIACET), 118 Route de Narbonne, F-31077 Toulouse Cedex, France*

We examine in this work the potential and the functional to be used in a density functional theory approach in order to describe correctly the formation and migration energies of monovacancies in nickel. As the formation enthalpy is not well-known experimentally at 0 K, we choose in a first step to determine some structural, magnetic, and elastic properties of the bulk, which are well-established experimentally. The comparison between both approaches, i.e., the local spin density approximation (LSDA) and the generalized gradient approximation (GGA) exchange-correlation functionals is analyzed. We conclude that the contribution of nonlocal GGA terms in order to describe correctly the electronic density is necessary to determine the formation and migration enthalpies and activation energy of monovacancy. The calculated formation H_v^f and migration H_v^m enthalpies differ significantly between both approaches. The overestimation of the LSDA approximation is of 0.25 eV for H_v^f and of 0.23 eV for H_v^m with respect to the GGA one, leading to a gap of 0.48 eV between both methods for the activation energy Q_1. We show that the GGA results are comparable with experimental data if the thermal expansion contribution is taken into account through the lattice parameter variation. Finally, it is shown that the activation energy is nearly independent of the thermal expansion effects; thus we can expect that the curvature of the Arrhenius plot of the diffusion factor near the melting point is essentially due to the contribution of divacancies.

DOI: 10.1103/PhysRevB.74.064111 PACS number(s): 71.15.Mb, 61.72.Ji, 61.72.Bb, 82.60.Cx

I. INTRODUCTION

Exposure of Ni-base alloys to oxidizing gaseous or aqueous environments at high temperatures is frequently associated to a degradation of the mechanical properties of the material. In many cases, this drop of mechanical properties cannot be simply attributed to the reduction of the metallic bearing section due to the oxidation process, i.e., alloy consumption. When an oxide grows by the outward diffusion of cations, which is the case for NiO formed on nickel base alloys, fresh oxide is formed at the gas (or water)–oxide scale interface. Metallic vacancies are then created at the metal–oxide scale interface. In a previous paper[1] it was demonstrated that a few parts of these defects diffuse far enough in the substrate to promote deleterious or unexpected effects on the mechanical properties of nickel base alloys. Thus the study of the stability of these vacancies as well as the supersaturation compared to the thermal equilibrium is necessary to better understand macroscopic properties of these alloys.

The goal of this paper is to determine the energetic properties of monovacancies (formation and migration enthalpies as well as activation energy). The major difficulty is selecting the theoretical approach which is more appropriate to resolve this problem. Indeed, many experimental and theoretical data of the monovacancy formation H_v^f and migration H_v^m enthalpies are available in the literature and exhibit strong disagreements. A lot of positron annihilation experiments are available[2–13] which give values varying from 1.54 to 1.80 eV. Other measurement techniques based on the specific heat of metals at high temperature, thermal expansion at high temperature, or electrical resistivity of metals are also available[14–17] with data varying from 1.4 to 1.6 eV. Theoretically, many various approaches are also available. They can be partitioned into two groups corresponding to first-principles local spin density approximation (LSDA)[18–21,26,27] or generalized gradient approximation (GGA)[26,27] approaches and various semi-empirical methods[21–25] as molecular statics and dynamics calculations,[28,29] lattice statics model,[30] or embedded atoms methods (EAM and MEAM).[31,32] LDA or LSDA calculations lead to values ranging from 1.77 to 1.81 eV. Semiempirical methods as well as first-principles calculations including GGA corrections give results which vary between 1.42 and 1.56 eV. The large disagreement between theoretical data lie in the different techniques (first-principles or semiempirical) and in different approximations within similar first-principles approaches (LDA or GGA, inclusion or not of lattice relaxations, etc.). Calculated and experimental data for the migration enthalpy H_v^m are less prolific. Experimental data are obtained indirectly from activation energy Q_1 measurements leading to H_v^m values ranging from 1.01 to 1.48 eV.[8,11,16,33,34] To our knowledge, only one theoretical calculation is available with a value of 0.97 eV.[28] Self-diffusion energies are comprised between 2.77 and 2.95 eV experimentally[8,16,33–37] and between 2.53 and 2.98 eV, theoretically.[28,32,38,39] Numerous experimental data for H_v^f, H_v^m, and Q_1 obtained with various techniques may be found in the report of Kraftmakher.[40] Concerning H_v^f, the comparison between experimental and theoretical results are very meaningful; Table I summarizes some experimental (positron annihilation and others) and

TABLE I. Some experimental and theoretical data values of the vacancy formation enthalpy in nickel. All values are in eV.

	Experimental		Theoretical
Positron annihilation	1.72±0.1 (Ref. 2), 1.74±0.06 (Ref. 3), 1.45±0.07 (Ref. 4), 1.55±0.05 (Ref. 5), 1.72 (Ref. 6), 1.54±0.15 (Ref. 7), 1.7 (Ref. 8), 1.80 (Ref. 9), 1.78 (Ref. 10), 1.79 (Ref. 11), 1.73 (Ref. 13)	LDA	1.76 (Ref. 19), 1.77 (Ref. 20), 1.78 (Ref. 21), 1.81 (Refs. 27)
Other measurements	1.6±0.1 (Ref. 14),[a] 1.58−1.63±0.05 (Ref. 15),[a] 1.46–1.55 (Ref. 16),[b] 1.4±0.2 (Ref. 17)[b]	Other calculations	1.54 (Ref. 27),[c] 1.56 (Refs. 23 and 29[c,d]), 1.57 (Ref. 24),[d] 1.46 (Ref. 25),[d] 1.31 (Ref. 26),[d] 1.58 (Ref. 28),[e] 1.28 (Ref. 30),[d] 1.42 (Ref. 31),[d] 1.51 (Ref. 32),[d] 1.35 (Ref. 33),[d] 1.33 (Ref. 34)[d]

[a]Quenching.
[b]Electrical resistivity.
[c]GGA.
[d]Semiempirical.
[e]Molecular dynamics.

theoretical (LDA and others) values of H_v^f. It shows that the LDA approaches are very close to the positron annihilation data, while GGA and other methods are close to the other experiments results. Such a result may be surprising because it is well-established now that annihilation positron experiments are the more reliable, while LDA calculations are known to overestimate significantly energetic values. In order to decide between the theoretical LDA or GGA which is the most reliable method to describe energetic properties of monovacancies, we have compared the capability of both methods to describe the experimentally well-known geometric, elastic, energetic, and magnetic properties of the bulk nickel. A lot of experimental data are available for the lattice parameter a_0 (6.65 au),[42,43] the bulk modulus B (186 Gpa),[41,42,44–46] the cohesion energy E_{coh},[41,42] and the magnetic moment μ (0.60 μ_B).[41,43,47] Furthermore, many theoretical results exist in the literature at the LDA (a_0,[27,48–58] B,[20,48–55,57,58] E_{coh},[48,57] μ[48–54,56–58]) and GGA (a_0,[27,48,49,51,53–55,57–59] B,[48,49,51,53–55,57–59] E_{coh},[48,57,59] and μ[49–51,57]) levels. The layout of this paper is as follows; in Sec. II, the computational details are described; results are presented in Sec. III; finally, we propose our conclusions in Sec. IV.

II. METHODS OF CALCULATION

The present calculations are done within the DFT formalism and the pseudopotential approximation. They are performed by means of the Vienna *ab initio* simulation program (VASP) developed at the Institut für Materialphysik of the Universität Wien.[60,61] The spin-polarized self-consistent Kohn-Sham equations are solved within the projected-augmented wave (PAW) method.[62,63] This leads to a powerful efficiency concerning the computation time. Two kinds of pseudopotentials have been tested at the LDA and GGA levels. They use the functional of Ceperley and Alder[64] parametrized by Perdew and Zunger.[65] For the second one the Perdew-Wang 91 functional (PW91)[66] is used to describe the exchange correlation effects. Concerning the computational parameters, the plane-wave energy cutoff is fixed to 14.7 Ry (400 eV) for all calculations independently of the size of the unit cell. On the other side, $4\times4\times4$ and $6\times6\times6$ Monkhorst-Pack[67] meshes are used to sample the Brillouin zone in the reciprocal space, depending on the size of the studied unit cell. The determination of the cohesive energy is obtained as being the difference between the energy of the isolated nickel and that of the bulk per unit atom. Thus we had to determine the energy of the nickel atom and more particularly the polarization and broken symmetry contribution, since the reference energy used in VASP concerns the nonpolarized case. These contributions allow one to describe the triplet nature of the ground state. Nevertheless this improvement is not sufficient because the DFT approach is inefficient to describe the "true" ground triplet state corresponding to the $4s^23d^8$ configuration; indeed, this latter must have a multireferential character in order to be an eigenstate of the total kinetic moment $J=L+S$; DFT only works with a single determinant.[68] In fact the monoreferential $4s^23d^8(^3F)$ triplet corresponds to three eigenstates states corresponding to $J=2$, 3, and 4 whose energies are 0, 0.165, and 0.275 eV, respectively.[69] Thus we can expect that the DFT calculated cohesive energy will be overestimated by 0.1–0.3 eV. To determine the formation and migration enthalpies of monovacancy, several sizes of fcc primitive cells were tested, i.e., 8, 32, 72, and 108 lattice sites per unit cell, in order to minimize the nearest-neighbor vacancy interactions. We decided that the size dependency is converged when both H_v^f and H_v^m do not vary more than 0.01 eV. In each case we take into account the lattice relaxation for both formation and migration enthalpy calculations. The relaxation is introduced by using a conjugate-gradient algorithm for formation enthalpies and all ions were allowed to relax. At the saddle point

TABLE II. Ground state structure characteristics and theoretical strengths calculated within the GGA and LSDA approaches. Here, a_0 is the equilibrium lattice parameter, B is the bulk modulus, μ is the magnetic moment per atom, σ_{max} is the strength (maximum stress), and E_{coh} the cohesion energy per atom.

Property	LDSA	GGA	Other	Experiment[c]
a_0 (a.u.)	6.474	6.656	6.50/6.67[a]	
			6.47/6.74[b]	6.65
B (Gpa)	280.6	195.1	255/195[a]	
			269/186[b]	186
$\mu(\mu_B)$	0.598	0.607	0.59/0.51[a]	
			0.56/0.61[b]	0.61
σ_{max} (Gpa)	37.5	29.0	39.5/27.4[b]	
E_{coh} (eV)	5.92	4.82 (4.67)[d]	6.09/4.93[a]	4.44

[a]Reference 53. Both numbers correspond to spin polarized LSDA and GGA results, respectively.
[b]Reference 58. Both numbers correspond to spin polarized LSDA and GGA results, respectively.
[c]Reference 43.
[d]Includes the qualitative correction due to the multireferential character of the Ni atom (see text).

corresponding to the migration enthalpy, first and second nearest neighbors of the migrating atom were allowed to move. The thermal expansion contribution to H_v^f, H_v^m and thus to Q_1 is estimated by studying their dependency with respect to the lattice parameter a. H_v^f, H_v^m, and Q_1 were calculated for five values of the lattice parameter a and fitted to a polynomial of degree two.

III. RESULTS

A. Structural, elastic, and magnetic properties of the bulk nickel

In Table II computational results concerning the bulk parameter a_0, the cohesive energy E_{coh}, the magnetic moment μ, the maximum stress σ_{max}, and the bulk modulus B are given. The GGA calculated bulk parameter is closed to the experimental data (less than 0.1%) while the local approach underestimates a_0 by 2.5%. Our calculated parameters are in complete agreement with previous calculations[53,58] at the LSDA and GGA levels, respectively.

The cohesive energies in each theoretical approach are overestimated, more particularly at the local level. The contributions of both the spin polarization and broken symmetry enhance by 0.58 and 0.63 eV the local and GGA approximations, respectively. Finally, the difference with experiment is significant in GGA (8%) and dramatic in LSDA (33%). As explained above, the monoreferential description of the wave function of the isolated nickel atom overestimates the energy by nearly 0.2 to 0.3 eV. Taking into account this correction, the GGA approach leads to a cohesive energy of nearly 4.50–4.60 eV which is not bad compared to the experimental value while the local approach remains unsatisfactory. The maximum stress is calculated from the dependence of the total energy per atom E_{tot} on the atomic volume V. The applied stress σ at any V can be determined according to the relation[70]

$$\sigma = \frac{dE_{tot}}{dV}. \tag{1}$$

It takes its maximum σ_{max} at the point inflection of the curve $E_{tot}(V)$. No experimental data are available for σ_{max}, but our results are comparable to other theoretical estimations done at the LSDA and GGA levels.[58]

The bulk modulus B is obtained from

$$B = V\frac{d^2E_{tot}}{dV^2}_{V=V_0}, \tag{2}$$

where V_0 is the atomic volume at the equilibrium state. Our nonlocal GGA results differ from experimental data by only 5% while the local LSDA approach overestimates B by nearly 50%. One more time, our values are comparable to previous recent calculations.[54,58] Finally, the calculated μ values are comparable to previous theoretical works,[54,58] and both LSD and GGA approaches reproduce experimental values. To summarize, various properties of the bulk nickel are well-described at the GGA level of calculation; on the contrary, the LSDA approximation systematically (i) underestimates the a_0 lattice parameter and (ii) overestimates strongly the cohesion energy as well as the bulk modulus. Furthermore, all our estimations at both the LSDA and GGA levels are closed to previous calculations showing that the PAW pseudopotentials are well-adapted to our study. Thus we shall rely preferably on the GGA results for the determination of monovacancy properties.

B. Formation and migration energies of a monovacancy at 0 K

1. Variation of H_v^f, H_v^m, and Q_1 with the size of the unit cell

The formation enthalpy of a vacancy H_v^f is given by

$$H_v^f = E_v^f - pV_v^f, \tag{3}$$

where E_v^f is the formation energy of the monovacancy; p is the external pressure applied to the solid, and V_v^f the formation volume of the monovacancy. This latter term is significant only for pressure of several kBar; thus in the following H_v^f will be equivalent to E_v^f because all the calculations are done at zero pressure. If N is the number of lattice sites of the supercell containing $N-1$ atoms when a monovacancy is incorporated, H_v^f can be calculated as

$$H_v^f = E_f(1,\Omega_1) - \frac{N-1}{N}E(0,\Omega_0), \tag{4}$$

where $E_f(1,\Omega_1)$ is the total energy of the supercell with $N-1$ atoms and one monovacancy located on a stable site at a relaxed unit cell volume Ω_1 and $E(0,\Omega_0)$ the total energy of the supercell with N atoms at a relaxed unit cell volume Ω_0. The migration enthalpy of the vacancy can be expressed as

$$H_v^m = E_m(1,\Omega_2) - E_f(1,\Omega_1), \tag{5}$$

where $E_m(1,\Omega_2)$ is the total energy of the supercell with $N-1$ nickel atoms and one monovacancy located on a saddle

TABLE III. Formation and migration enthalpies (in eV) and activation energy of the vacancy defect for various sizes of the initial supercell at the local LSDA and nonlocal GGA levels. Nonrelaxed and relaxed values are presented.

	H_v^f		H_v^m		Q_1	
Size	LSDA	GGA	LSDA	GGA	LSDA	GGA
			Nonrelaxed			
8	1.663	1.367	1.531	1.318	3.194	2.685
32	1.744	1.443	1.814	1.580	3.558	3.023
72	1.725	1.432	1.808	1.578	3.533	3.010
108	1.717	1.428	1.798	1.571	3.516	2.999
			Relaxed			
8	1.575	1.285	1.312	1.146	2.887	2.431
32	1.656	1.378	1.479	1.263	3.135	2.641
72	1.636	1.363	1.504	1.296	3.140	2.659
108	1.621	1.370	1.513	1.285	3.134	2.655

site between two stable sites at a relaxed unit cell volume Ω_2. Finally, the activation energy Q_1 is calculated as

$$Q_1 = H_v^f + H_v^m \tag{6}$$

or from Eqs. (4) and (5):

$$Q_1 = E_m(1,\Omega_2) - \frac{N-1}{N}E(0,\Omega_0), \tag{7}$$

which shows that Q_1 depends only of the migration energy of the vacancy; more particularly, as shown below, the relaxation contribution of the lattice to Q_1 is equal to that of H_v^m. In Table III the vacancy parameters (formation, migration, self-diffusion enthalpies) from our first principles calculations are given at both the LSDA and GGA levels, together with the effect of the variation of the supercell size. The nonrelaxed results are obtained with the optimized lattice parameters of the bulk for both approaches. Furthermore, the effects of the lattice relaxation due to the presence of the monovacancy are given. Various unit cells including a monovacancy are represented in Fig. 1. First, the convergence of H_v^f is nearly reached for 32 lattice sites, the change when growing to 72 lattice sites being less than 0.01 eV at the relaxed and nonrelaxed levels. On the other side, the convergence of H_v^m is slower and needs a 72 site unit cell to be well-described. This is true independently of the chosen method (LSDA or GGA); the change between 32 and 72 sites (0.03 eV) is essentially included in the relaxation contribution to H_v^m. There is no significant changes between 72 and 108 sizes. The size of 32 lattice sites corresponds to a vacancy-vacancy distance of 13.3 a.u., showing that the long range vacancy-vacancy interaction is small, but that the relaxation effects related to the saddle point during the vacancy migration are still constricted. At the converged values (72 or 108 unit cell sites) we show that the relaxation effects on the formation enthalpy are small and comparable at the LSDA and GGA levels (less than 0.1 eV). However, the effect is more significant for the migration enthalpy (nearly 0.35 eV) due essentially to a stronger repulsion energy between the migrating nickel atom and its first nearest neighbors at the saddle point; on the other side, the relaxation contribution of the second nearest neighbors is very small (less than 0.03 eV).

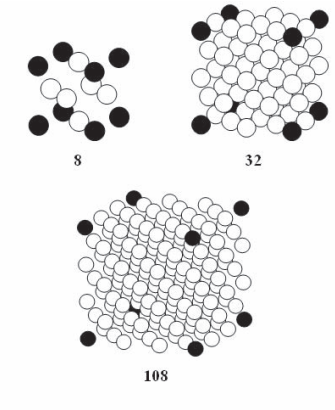

FIG. 1. Unit supercells including 8, 32, and 108 nickel atoms. Vacancy positions are represented by closed circles and nickel atoms by open circles.

2. Comparison between LSDA and GGA results

Table IV shows H_v^f, H_v^m, and Q_1 calculated at the LSDA and GGA levels, together with experimental positron annihilation data. Fig. 2 visualizes the GGA results. Comparisons for both H_v^f and H_v^m show discrepancies approaching 0.3 eV between both types of calculations. This leads to an overestimation of the LSDA Q_1 value of nearly 0.5 eV with respect to the GGA ones. Concerning H_v^f, comparison with experiment shows that the annihilation positron data are best reproduced by the LDA calculations, while GGA results are more close to other experimental measurements (see Table I). The annihilation positron data are known as more reliable; it is thus tempting to consider the LSDA as a better approach to study energetic properties of monovacancies. This appears in

TABLE IV. Comparison of our results with the most recent experimental and theoretical energetic properties of a monovacancy in nickel. Absolute lattice relaxation contributions are given in parentheses

	This work		Other works	
	LSDA	GGA	Theoretical	Experimental
H_v^f	1.621 (0.097)	1.370 (0.058)	1.54,[a], 1.42[b]	1.73,[c], 1.79[d]
H_v^m	1.513 (0.382)	1.285 (0.344)	0.97[e]	1.04[c]
Q_1	3.134 (0.382)	2.655 (0.344)	2.53[e]	2.78[c]

[a]GGA, Ref. 27.
[b]Embedded atom method, Ref. 31.
[c]Positron annihilation, Ref. 12.
[d]Positron annihilation, Ref. 11.
[e]Molecular statics, Ref. 28.

the literature where numerous LSDA approaches are available contrary to the GGA ones. Nevertheless, the calculated Q_1 activation energy is overestimated by the LSDA result compared to experimental values (see Table IV). The GGA approach in this case seems much better. At this instant of our discussion we must mention the work of Carling *et al.*[71] He showed that the GGA fails to reproduce formation enthalpies in aluminum, due to correlation effects near electronic edges. An empirical correction was introduced for this deficiency. Such an effect has been taken into account by Andersson *et al.*[72] in copper. If we consider that the contribution in nickel is of the same order as that in copper (0.05 eV) ($3d$ valence electrons in both atoms) we can consider that the H_v^f and Q_1 calculated at the GGA level are 1.42 and 2.70 eV. At the LSDA level, we may expect that the correction is slightly lower as found by Carling *et al.*[71] in aluminum. As seen in Table I, the various estimations of the formation enthalpy H_v^f are comprised between nearly 1.4 and 1.8 eV and thus seem to be significantly dependent of the temperature (the experimental measurement conditions vary strongly depending on the nature of the experience). Our calculated values at 0 K of H_v^f are thus difficult to compare with high temperature experimental data. On the other hand the comparison of calculated Q_1 at the LSDA (3.15 eV) and GGA (2.70 eV) with experimental data (2.8 eV) shows that the GGA approach seems more efficient to determine the activation energy. So the good agreement of the LSDA result with experimental data concerning the formation enthalpy may be fortuitous. In order to introduce the temperature effects, we decided to analyze the influence of the lattice parameter changes on H_v^f, H_v^m, and Q_1 in order to improve our study which until now does not take into account the thermal expansion due to the temperature. As mentioned above, experimental results obtained from positron annihilation techniques are performed in temperature ranges for which fcc Ni is found to be paramagnetic ($\sim$1600 K while the Curie temperature T_c=627 K). Therefore for temperatures higher than T_c we completed our study by spin-nonpolarized calculations [nonmagnetic (NM) phase]. The problem with this choice to describe a paramagnetic (PM) phase is that the PM state consists of randomly disordered local magnetic moments, but not in the sense of locally compensated spins as in the NM phase. In fact we cannot model the PM phase with conventional periodic DFT and colinear spins. The choice of the NM description leads one to describe each Ni atom in a new configuration state ($3d^9 4s$) corresponding to the ^1D excited atomic level and thus with a different electronic density. Thus we think that the FM state is better to describe the PM one in the sense that the individual electronic densities are the same in both phases, the energetic difference between them being essentially due to magnetic interactions, i.e., the exchange energy between the two spins $\vec{S}_i$ and $\vec{S}_j$ (Heisenberg model):[41]

$$U = -2J\vec{S}_i\vec{S}_j, \tag{8}$$

where J is the exchange integral related to the overlap between the charge distributions of atoms i and j. We can establish an approximate relation for J related to an atom by taking into account only its nearest neighbors:[41]

$$J = \frac{3k_B T_c}{2zS(S+1)} \tag{9}$$

where k_B is the Boltzmann constant, T_c the Curie temperature, z the number of nearest neighbors, and S the spin of the

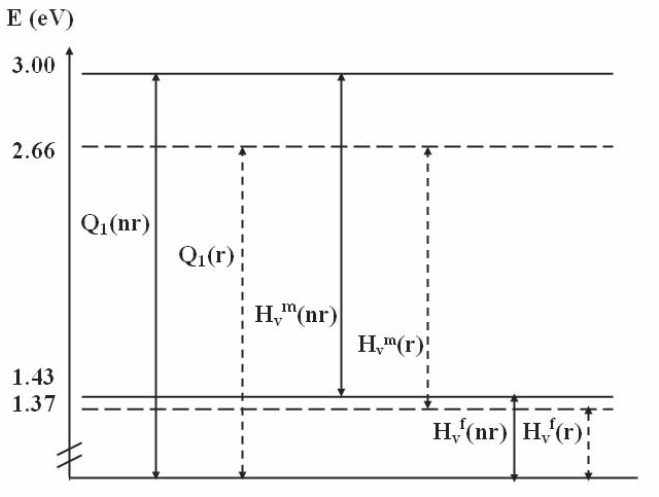

FIG. 2. Energetic scheme of the formation H_v^f and migration H_v^m enthalpies and activation energy Q_1, with (r) and without (nr) lattice relaxation. The reference energy is $(N-1)/NE(0,\Omega_0)$.

atom. Applying the Heisenberg model to the Ni atom, $J=0.003$ eV with $S=1$, $T_c=627$ K, and $z=12$, which shows that the magnetic contribution to the total atomic energy is very small.

C. Effects of the anharmonic contribution of the temperature: Thermal expansion

Dilatation of metals is due to the contribution of anharmonic terms contained in the interaction potential. Thermal expansion is used in order to determine the formation enthalpies of vacancies, like, for example, in dilatometry methods (linear extrapolation, modulation, or differential dilatometry experiments). The principle is that the vacancy formation leads to an increase in the volume of the solid and in the thermal expansivity at high temperatures. The problem now is to know if formation and migration enthalpies as well as the self-diffusion process depend or not on the temperature and thus on the thermal expansion. Starting from the thermodynamic relation:

$$\left(\frac{\partial H_v^f}{\partial T}\right)_P = T\left(\frac{\partial S_v^f}{\partial T}\right)_P, \tag{10}$$

where S_v^f is the entropy formation; we can expect that the relaxation of the atoms around vacancy increases with the lattice parameter a_0 and thus with the thermal expansion; the formation entropy S_v^f must thus increase with temperature, as well as the formation enthalpy. On the contrary, we may expect that migration energy decreases with thermal expansion; indeed, H_v^m depends of both $E_f(1,\Omega_1)$ and $E_m(1,\Omega_2)$ [see Eq. (5)]; both energies increase with the lattice parameter; on the other hand we can expect that the increasing of $E_m(1,\Omega_2)$ is less important due to a larger weakening of the nickel-nickel ion repulsion energy at the saddle point position. The dependency of the self-diffusion with thermal expansion is less clear. It is known that nickel exhibits a slight upward curvature in the Arrhenius plot of the tracer self-diffusion coefficient. Principally two mechanisms can be involved in that case. First, the self-diffusion process involves only a monovacancy mechanism. In that case, the coefficient of self-diffusion is given by

$$D = D_0 \exp - \frac{Q_1}{k_B T}, \tag{11}$$

where

$$D_0 = a_0^2 f \nu g \exp - \frac{S_v^f + S_v^m}{k_B} \tag{12}$$

is the preexponential factor. Here a_0 is the lattice parameter, f is the correlation factor of monovacancies, ν is the frequency associated to the jump of atoms into adjacent vacancies, g is a geometrical factor, and S_v^f and S_v^m are the entropy of vacancy formation and migration. Q_1 is the activation energy for monovacancy defined in Eqs. (6) and (7). In that case, the curvature in the tracer Arrhenius plot is explained by an activation energy Q_1 and entropy $S_1=S_v^f+S_v^m$ dependencies on temperature.[33,73,74] Second, the contribution of more than one diffusion mechanism (essentially divacancy diffusion) has been involved.[28,33,34,75] With this approach, the coefficient of self-diffusion obeys the equation

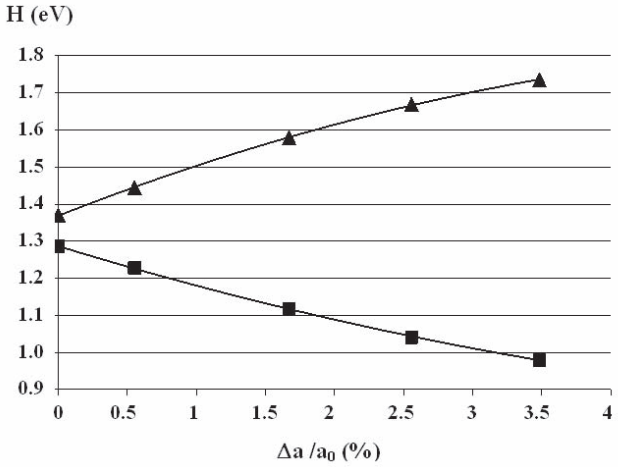

FIG. 3. Relative linear expansion dependence of formation H_v^f (▲) and migration H_v^m (■) enthalpies.

$$D = D_0 \exp - \frac{Q_1}{k_B T} + D_{02} \exp - \frac{Q_2}{k_B T}, \tag{13}$$

where the activation energies Q_1 and Q_2 are independent of the temperature as well as the preexponential factors D_0 and D_{02}. This second mechanism may be available if divacancies are present in the lattice crystal at high temperature. In that case, their contribution to self-diffusion is likely since their diffusion is easier than the diffusion of monovacancies. Finally, we must mention that the contribution of multiple vacancy jumps[76,77] has also been involved. As our work is concerned with monovacancies properties, we will focus on the possible validity of the first proposed mechanism, i.e., is their a dependency or not of Q_1 (and thus S_1) with the temperature? For this purpose, we present in Fig. 3 the variations of H_v^f and H_v^m with the linear expansion (in percent) of the bulk lattice parameter a_0. H_v^f and H_v^m have been fitted by a polynomial of degree two from the calculated points shown in Fig. 3. As suggested above, H_v^f is increasing with $\Delta a/a_0$ while H_v^m decreases. Their analytical expression is

$$H_v^f = -0.0117\left(\frac{\Delta a}{a_0}\right)^2 + 0.1463\left(\frac{\Delta a}{a_0}\right) + 1.369, \tag{14}$$

$$H_v^m = 0.0072\left(\frac{\Delta a}{a_0}\right)^2 - 0.1135\left(\frac{\Delta a}{a_0}\right) + 1.286, \tag{15}$$

which leads to a very small increasing of Q_1 with respect to $\Delta a/a_0$:

$$Q_1 = -0.0045\left(\frac{\Delta a}{a_0}\right)^2 + 0.0328\left(\frac{\Delta a}{a_0}\right) + 2.655. \tag{16}$$

We may expect that the behavior of H_v^f, H_v^m, and Q_1 with respect to the temperature is similar.

TABLE V. Thermal expansion effects on the vacancy formation, migration, and activation energies (in eV) at the spin-polarized (FM) and spin-nonpolarized (NM) levels. α is the linear coefficient of thermal expansion. Results obtained in GGA with a 108 sites unit cell size.

$\Delta a/a_0$ (%)	$\alpha(10^{-6}\ \mathrm{K}^{-1})$	T (K)	Spin	H_v^f	H_v^m	Q_1
0	0	0	FM	1.370	1.285	2.655
0.114	13.1	293	FM	1.386	1.273	2.659
2.370	23.22	1600	FM	1.660	1.049	2.709
			NM	1.666	0.936	2.602
2.674	24.22	1728	FM	1.687	1.026	2.713
			NM	1.694	0.913	2.607

The problem is now to give correspondence between the lattice parameter and the temperature. Recently, Lu *et al.*[78] determined thermal expansion of nickel by means of the Calphad approach in order to obtain a reasonable description of experimental data.[79,80] All data are very similar. The dependency of the linear coefficient energy α with T is also proposed in an analytical form by Glazkov.[17] In order to estimate the temperature corresponding to $\Delta a/a_0$, we used the analytical form proposed by Suh *et al.*[80] where the thermal expansion was measured by the dilatation method as well as by x-ray diffraction. We obtain H_v^f, H_v^m, and Q_1 from Eqs. (14)–(16) for some characteristic values of T: $T=293$ K corresponding to the room temperature, $T=1600$ K which is the mean value used in the positron annihilation experiments, and $T=1728$ K which corresponds to the melting point of nickel. For each temperature, the linear coefficient of thermal expansion α is determined. All results are summarized in Table V. First, the estimated value of H_v^f becomes closed to the positron annihilation experimental data at $T=1600$ K. Taking into account the empirical corrections proposed by Carling[71] we obtain at this temperature $H_v^f \sim 1.71$ eV and $Q_1 \sim 2.81$ eV. Hence the contribution of temperature through thermal expansion to various energetic properties of monovacancies at the GGA level reproduce reasonably experimental data. The more significant result is that Q_1 increases very slightly with T ($\sim +0.05$ eV from 0 to 1600 K). Thus we may expect that the deviation of the Arrhenius plot at high temperature cannot be attributed to the temperature dependency of Q_1. Indeed from Eq. (10) we deduce that D_0 given in Eq. (12) is constant and that the expression of D in Eq. (11) leads to a linear relation between $\ln(D)$ and $(1/T)$ giving a linear Arrhenius plot. As it is not the case experimentally, we can suggest that more than one diffusion mechanism is involved in the self-diffusion process; the simplest expression of D is given by Eq. (13) which takes into account the contribution of divacancies to the self-diffusion process; indeed Eq. (13) shows that in this case, $\ln(D)$ is no longer a linear function of $1/T$. Finally, we give in Table V the enthalpies and energies calculated with the spin-nonpolarized (NM) approach for temperatures higher than T_c. Although the electronic distribution of the individual atoms in that case are not those corresponding to the FM or PM phases (see Sec. III C), we see that H_v^f remains nearly unchanged while H_v^m and thus Q_1 decreases slightly at 0.11 eV, due to a larger overlap of the electronic density of the migrating atom with its nearest neighbors.

IV. CONCLUSION

Some geometric, elastic, and magnetic properties of the bulk and 0 K temperature estimation of H_v^f, H_v^m, and Q_1 have been calculated directly from first-principles at the LSDA and GGA levels. The bulk properties are well-reproduced with the PAW pseudopotentials when the GGA approach is used, while LSDA leads to a strong overestimation of bulk modulus, cohesion energy and to an underestimation of the bulk lattice parameter. From this, the calculated formation and migration enthalpies and activation energy of the self-diffusion at the GGA level were those compared with experimental data. Our results show a strong underestimation of H_v^f of nearly 0.4 to 0.5 eV compared with most reliable experiments using positron annihilation techniques. The discrepancy is not surprising since our 0 K temperature results cannot be directly compared with experimental values generally obtained by techniques which arise at temperatures close to the melting point. In order to take into account the temperature effects, we studied the dependency of H_v^f, H_v^m, and Q_1 with respect to the lattice parameter. This is an approach which allows one to take into account the thermal expansion of the bulk due to the anharmonicity of the lattice vibrations. Our results show that the formation and migration enthalpies are strongly correlated to the a value. More particularly H_v^f increases until values comparable with experimental data, when a corresponds nearly to temperatures closed to the melting point. Furthermore, it is shown that the activation energy is nearly independent of a and has a value comparable with various theoretical and experimental determinations. We can conclude that the deviation to the Arrhenius plot of the diffusion coefficient in nickel in the range of high temperature is rather due to the formation and diffusion of divacancies. The study of formation, diffusion, and stability of divacancies in nickel is the next goal of our work.

ACKNOWLEDGMENTS

Computer resources for this job were provided by

CALMIP (Toulouse, France) and the computer center GRID'5000 Nation-Wide Grid Experimental platform funded by the French Ministery of Research through the ACI GRID Program. We are grateful to Irea Touche (supported by INPT) for gridifying our codes. The calculations have been performed using the *ab initio* total-energy program VASP developed at the Institut für Materialphysik of the Universität Wien, Austria.

*Electronic address: claude.mijoule@ensiacet.fr

[1] S. Pérusin, B. Viguier, D. Monceau, L. Ressier, and E. Andrieu, Acta Mater. **52**, 5375 (2004).
[2] S. Nanao, K. Kuribayashi, S. Tanigawa, and M. Doyama, J. Phys. F: Met. Phys. **7**, 1403 (1977).
[3] J. L. Campbell, C. W. Schulte, and J. A. S. Jackman, J. Phys. F: Met. Phys. **7**, 1985 (1977).
[4] H. Matter, J. Winter, and W. Triftshäuser, Appl. Phys. **20**, 135 (1979).
[5] K. Maier, M. Peo, B. Saile, P. Valenta, H. Schaefer, and E. Seeger, Philos. Mag. A **40**, 701 (1979).
[6] K. G. Lynn, C. L. Snead, and J. J. Hurst, J. Phys. F: Met. Phys. **10**, 1753 (1980).
[7] R. W. Siegel, Annu. Rev. Mater. Sci. **10**, 393 (1980).
[8] L. C. Smedskjaer, M. J. Fluss, D. G. Legnini, M. K. Chason, and R. W. Siegel, *Positron Annihilation*, edited by P. G. Coleman, S. C. Sharma, and L. M. Diana (North-Holland, Amsterdam, 1982).
[9] H.-E. Schaefer, Phys. Status Solidi A **102**, 47 (1987).
[10] H. Schultz and P. Ehrhart, *Atomic Defects in Metals*, edited by H. Ullmaier, Landolt-Börnstein, New Series, Group III (Springer, Berlin, 1991).
[11] *Atomic Point Defects in Metals: Crystal and Solid State Physics*, edited by H. Ullmaier, Landolt-Börnstein (Springer-Verlag, Berlin, 1991), Vol. 25, pp. 211–214.
[12] J. Wolff, M. Franz, J.-E. Kluin, and D. Schmid, Acta Mater. **45**, 4759 (1997).
[13] G. Dlubek, O. Brümmer, and N. Meyendorf, Phys. Status Solidi A **39**, K95 (1977).
[14] A. A. Mamalui, T. D. Ositinskaya, V. A. Pervako, and V. I. Khotkevich, Sov. Phys. Solid State **10**, 2290 (1968).
[15] W. Wycisk and M. Feller-Kniepmeier, Phys. Status Solidi A **37**, 183 (1976).
[16] W. Schüle and R. Scholz, *Point Defects and Defect Interactions in Metals*, edited by J. Takamura, M. Doyama, and M. Kiritani (Univ. Tokyo Press, Tokyo, 1982), p. 257.
[17] Y. Glazkov, High Temp. **25**, 51 (1987).
[18] U. Klemradt, B. Drittler, T. Hoshino, R. Zeller, P. H. Dederichs, and N. Stefanou, Phys. Rev. B **43**, 9487 (1991).
[19] P. H. Dederichs, T. Hoshino, B. Drittler, K. Abraham, and R. Zeller, Physica B **172**, 203 (1991).
[20] T. Korhonen, M. J. Puska, and R. M. Nieminen, Phys. Rev. B **51**, 9526 (1995).
[21] P. A. Korzhavyi, I. A. Abrikosov, B. Johansson, A. V. Ruban, and H. L. Skriver, Phys. Rev. B **59**, 11693 (1999).
[22] B. F. Kostromin, Y. M. Plishkin, I. E. Podchinyonov, and I. Sh. Trakhtenberg, Fiz. Met. Metalloved. **55**, 450 (1983).
[23] G. I. Ackland, G. Tichy, V. Vitek, and M. W. Finnis, Philos. Mag. A **56**, 735 (1987).
[24] U. Krause, J. P. Kuska, and R. Wedell, Phys. Status Solidi B **151**, 479 (1989).
[25] V. Rosato, M. Guillope, and B. Legrand, Philos. Mag. A **59**, 321 (1989).
[26] M. Asato, T. Hoshino, T. Asada, R. Zeller, and P. H. Dederichs, J. Magn. Magn. Mater. **177-181**, 1403 (1998).
[27] T. Mizuno, M. Asato, T. Hoshino, and K. Kawakami, J. Magn. Magn. Mater. **226-230**, 386 (2001).
[28] M. García Ortega, S. B. Ramos de Debiaggi, and A. M. Monti, Phys. Status Solidi B **234**, 506 (2002).
[29] M. de Koning, S. Ramos de Debiaggi, and A. M. Monti, Phys. Rev. B **70**, 054105 (2004).
[30] A. Ghorai, Phys. Status Solidi B **167**, 551 (1991).
[31] K. Sato, T. Yoshiie, Y. Satoh, Q. Xu, E. Kuramoto, and M. Kiritani, Radiat. Eff. Defects Solids **157**, 171 (2002).
[32] B.-J. Lee, J.-H. Shim, and M. I. Baskes, Phys. Rev. B **68**, 144112 (2003).
[33] A. Seeger and H. Mehrer, *Vacancies and Interstitial in Metals*, edited by A. Seeger, D. Schumacher, W. Schilling, and J. Diehl (North-Holland, Amsterdam, 1970), p. 1.
[34] H. Bakker, Phys. Status Solidi **28**, 569 (1968).
[35] K. Maier, H. Mehrer, E. Lessmann, and W. Schüle, Phys. Status Solidi B **78**, 689 (1976).
[36] M. Doyama and J. S. Koehler, Acta Metall. **24**, 876 (1976).
[37] C. J. Smithells, *Metals Reference Book*, 7th ed., edited by E. A. Brandes and G. B. Brook (Butterworth-Heinemann, Oxford, 1992).
[38] G. Neumann and V. Tölle, Philos. Mag. A **54**, 619 (1986).
[39] G. Neumann and V. Tölle, Philos. Mag. A **61**, 563 (1990).
[40] Y. Kraftmakher, Phys. Rep. **299**, 79 (1998).
[41] C. Kittel, *Introduction to Solid State Physics*, 7th ed. (Wiley, New York, 1996).
[42] C. J. Smithells, *Metals Reference Book*, 6th ed., edited by E. A. Brandes (Butterworths, London, 1983).
[43] *Handbook of Chemistry and Physics*, edited by D. R. Lide (CRC Press, Boca Raton, 1995).
[44] A. F. Guillermet and G. Grimvall, Phys. Rev. B **40**, 1521 (1989).
[45] P. Lazor and S. K. Saxena, Terra Nova **5**, 363 (1993).
[46] B. Chen, D. Penwell, and M. B. Kruger, Solid State Commun. **115**, 191 (2000).
[47] M. B. Stearns, Landolt-Börnstein, *New Series*, Vol. III/19a (Springer, Berlin, 1986).
[48] T. C. Leung, C. T. Chan, and B. N. Harmon, Phys. Rev. B **44**, 2923 (1991).
[49] M. Körling and J. Häglund, Phys. Rev. B **45**, 13293 (1992).
[50] J.-H. Cho and M.-H Kang, Phys. Rev. B **52**, 9159 (1995).
[51] J.-H. Cho and M. Scheffler, Phys. Rev. B **53**, 10685 (1996).
[52] M. J. Mehl and D. A. Papaconstantopoulos, Phys. Rev. B **54**, 4519 (1996).
[53] E. G. Moroni, G. Kresse, J. Hafner, and J. Furthmuller, Phys. Rev. B **56**, 15629 (1997).
[54] M. Asato, A. Settels, T. Hoshino, T. Asada, S. Blugel, R. Zeller, and P. H. Dederichs, Phys. Rev. B **60**, 5202 (1999).
[55] T. Hoshino, N. Papanikolaou, R. Zeller, P. H. Dederichs, M.

Asato, T. Asada, and N. Stefanou, Comput. Mater. Sci. **14**, 56 (1999).
[56] F. Starrost, H. Kim, S. C. Watson, E. Kaxiras, and E. A. Carter, Phys. Rev. B **64**, 235105 (2001).
[57] U. V. Waghmare, H. Kim, I. J. Park, N. Modine, P. Maragakis, and E. Kaxiras, Comput. Phys. Commun. **137**, 341 (2001).
[58] M. Černy, J. Pokluda, M. Šob, M. Friák, and P. Šandera, Phys. Rev. B **67**, 035116 (2003).
[59] M. I. Baskes, Mater. Chem. Phys. **50**, 152 (1997).
[60] G. Kresse and J. Hafner, Phys. Rev. B **47**, 558 (1993).
[61] G. Kresse and J. Furthmuller, Phys. Rev. B **54**, 11169 (1996).
[62] P. E. Blochl, Phys. Rev. B **50**, 17953 (1994).
[63] G. Kresse and D. Joubert, Phys. Rev. B **59**, 1758 (1999).
[64] D. M. Ceperley and B. J. Alder, Phys. Rev. Lett. **45**, 566 (1980).
[65] J. P. Perdew and A. Zunger, Phys. Rev. B **23**, 5048 (1981).
[66] J. P. Perdew and Y. Wang, Phys. Rev. B **46**, 12947 (1992).
[67] H. J. Monkhorst and J. D. Pack, Phys. Rev. B **13**, 5188 (1976).
[68] C. Daul, K. G. Doklo, and A. C. Stuckl, *Recent Advances in Density Functional Theory, Part II* (World Scientific, River Edge, NJ, 1997), p. 61.
[69] http://physics.nist.gov/cgi-bin/AtData/main-asd.
[70] P. Šandera, J. Pokluda, L. G. Wang, and M. Šob, Mater. Sci. Eng., A **234-236**, 370 (1997).
[71] K. Carling, G. Wahnstrom, T. R. Mattsson, A. E. Mattsson, N. Sandberg, and G. Grimvall, Phys. Rev. Lett. **85**, 3862 (2000).
[72] D. A. Andersson and S. I. Simak, Phys. Rev. B **70**, 115108 (2004).
[73] H. M. Gilder and D. Lazarus, Phys. Rev. B **11**, 4916 (1975).
[74] J. N. Mundy, Phys. Status Solidi B **144**, 233 (1987).
[75] N. L. Peterson, Comments Solid State Phys. **8**, 107 (1978).
[76] A. Da Fano and G. Jacucci, Phys. Rev. Lett. **39**, 950 (1977).
[77] G. De Lorenzi and F. Ercolessi, Europhys. Lett. **20**, 349 (1992).
[78] X. G. Lu, M. Selleby, and B. Sundman, CALPHAD: Comput. Coupling Phase Diagrams Thermochem. **29**, 68 (2005).
[79] M. Yousuf, P. Ch. Sahu, H. K. Jajoo, S. Rajagopalan, and K. Govinda Rajan, J. Phys. F: Met. Phys. **16**, 373 (1986).
[80] I.-K Suh, H. Ohta, and Y. Waseda, J. Mater. Sci. **23**, 757 (1988).